






Electromagnetically induced transparency in all-dielectric metamaterials: Coupling between magnetic Mie resonance and substrate resonance

Weiqi Cai , Yuancheng Fan ,* Xinchao Huang , Quanhong Fu, Ruisheng Yang , Wei Zhu, and Fuli Zhang †

Research and Development Institute in Shenzhen and Department of Applied Physics, School of Science, Northwestern Polytechnical University, Xian 710129, China



(Received 15 July 2019; published 4 November 2019)

We theoretically and experimentally studied the coupling of the magnetic Mie resonance of a dielectric cuboid and the guide mode resonance of an alumina slab in an all-dielectric metamaterial. It is found that the excitation of the discrete guide mode resonance or substrate resonance of the alumina slab can be properly controlled by designing the geometry of the dielectric cuboid. Moreover, it is found that the coupling of substrate resonance and the Mie resonance of the cuboid can be tailored to achieve electromagnetically induced transparency (EIT)-like spectrum. The tunability of the EIT-like spectrum based on the geometric parameters was also studied. Our results utilizing the crucial contribution of substrate derive a realization of EIT in all-dielectric metamaterial and thus pave a way for optical spectral control with all-dielectric coupled system.

DOI: [10.1103/PhysRevA.100.053804](https://doi.org/10.1103/PhysRevA.100.053804)

I. INTRODUCTION

Metamaterial [1–8], or its two-dimensional counterpart metasurface [9–12], is a class of artificial media composed of subwavelength-sized resonant elements. The resonant micro- and nanoelements, also called as meta-atoms, can be freely designed for optical properties unattainable in nature, which may play an important role in improving light-matter interactions for fundamental physics and applications [13–15]. Recently, the subwavelength meta-atoms of the metamaterials have been designed for the realization of exotic transport phenomena appearing in quantum systems. The classical analogies of quantum features in metamaterials can be employed to dramatically reduce the extreme conditions for observing quantum phenomena in experiments, which may stimulate the practical application of characteristic transport properties of quantum systems. Electromagnetically induced transparency (EIT) [16,17] was suggested as a technique for eliminating the effect of a medium on a propagating beam of electromagnetic radiation, which can be used to remove optical self-focusing and defocusing and to improve transmission through an opaque medium in a narrow window with low absorption and steep dispersion. The steep dispersion of EIT is promising for slow light and the enhanced light-matter interactions. However, the extreme environment requirement for quantum EIT obstructs it from practical applications. The spectral characteristics of EIT have been reproduced in several classical structures [18–28]. Zhang *et al.* demonstrated the EIT spectrum and steep dispersion in a direct manner with a plasmonic metamaterial composed of bright and dark meta-atoms [18]. Later, all-dielectric metamaterials [29–40] with

EIT-like spectra were fabricated for avoiding the Ohmic loss in metallic metamaterials.

In this work, we demonstrate an EIT-like spectrum of an all-dielectric metamaterial composed of a ceramic cuboid on an alumina substrate. Unlike previous studies on EIT with all-dielectric metamaterials, the dielectric substrate plays a dominant role in the formation of the EIT-like effect. It is found that the second-order bound state ($TE_{2,0}$) of the alumina substrate can be excited by the magnetic resonant of ceramic cuboid normal to the substrate [41–43]. Then the magnetic resonance of the ceramic particle can be tuned to approach the resonant mode of the alumina substrate, and the coupling between the magnetic Mie resonance and substrate resonance will induce a transparent window. The tunability of the EIT-like effect based on the geometric parameters was also studied. Our study demonstrates the important influence of the dielectric substrate on the electromagnetic properties of all-dielectric metamaterials.

II. RESULTS AND DISCUSSION

The designed all-dielectric metamaterial is schematically illustrated in Fig. 1(a). A dielectric cuboid is placed on top of an alumina slab, and the cross section (width $a = 22.86$ mm, height $b = 10.16$ mm) of the slab is the same as the waveguide of standard the X band, which is employed for the study of the all-dielectric metamaterial, and the position of the ceramic cuboid away from the center of slab along the x direction is p . We used a commercial electromagnetic solver based on the finite-difference-time-domain (FDTD) method for all the numerical simulations in our study.

The ceramic cuboid is made of calcium carbonate CaTiO_3 doped by 1 wt% ZrO_2 that processes with a relatively low loss (with dielectric constant $\epsilon = 123$ and loss tangent $\tan\delta = 0.001$) [36], and the dimensions of the cuboid are $3.5 \text{ mm} \times 3.5 \text{ mm} \times 1.0 \text{ mm}$. The ceramic cuboid is placed

*phyfan@nwpu.edu.cn

†fuli.zhang@nwpu.edu.cn

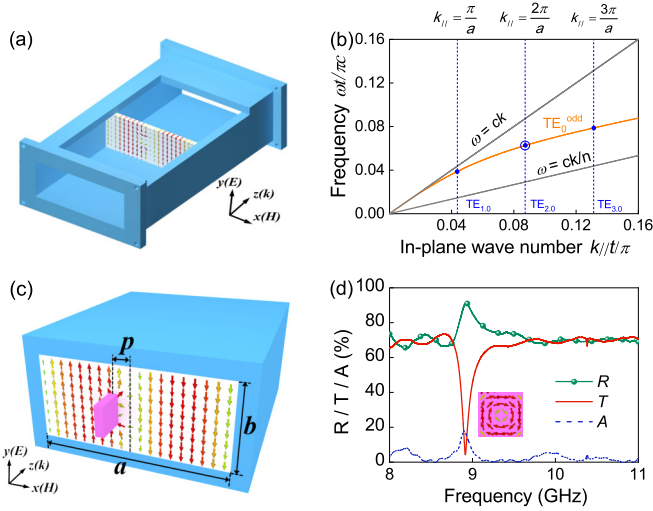


FIG. 1. (a) Schematic diagram of the waveguide and alumina slab. (b) The dispersion diagram of the $TE_0^{(odd)}$ mode of alumina slab; the blue dotted lines indicate different eigenmodes of alumina slab. (c) Schematic diagram of the waveguide and all-dielectric metamaterial made of $CaTiO_3$ cuboid and alumina slab. (d) Transmission, reflection, and absorption spectra of an all-dielectric metamaterial.

with its square cross section along the x direction to excite its first-order Mie resonance within the working band of the waveguide. First, we studied the electromagnetic behavior of a single ceramic cuboid by placing it at the center of the alumina slab, i.e., $p = 0$ mm. In the experiment, the transmission through the sample was measured with a vector network analyser (VNA, AV3629D) in the range of 8–12 GHz, and the measured result agrees well with our FDTD simulations. The measured transmission, reflection, and absorption spectrum of the single ceramic cuboid are shown in Fig. 1(d), from which we can see a sharp magnetic resonance around the frequency of 8.9 GHz. Distributions of the electric field on the cross sections of the ceramic cuboid are presented in Fig. 1(d) for understanding the resonant mechanism. As can be seen from the field distribution, the resonant mode of the ceramic cuboid shows the same picture as the base mode of spherical resonator, which is a magnetic mode. The on-resonance magnetic field of the mode is overlapped with the propagating electromagnetic waves in the waveguide, suggesting that the resonance is excited directly by the magnetic component of the incident electromagnetic wave.

The substrate of metamaterial is commonly chosen as a low-loss dielectric material for its insignificant influence on the resonant quality of micro- and nano-structured layers. Recently, the influence of the dielectric substrate on the overall properties of metamaterial has attracted more attention. For example, the infrequently studied dielectric substrate was exploited for sheet metamaterial with large quality factor [38]. The dielectric substrate supports a continuous dark bound state with respect to the incident light, and then the dielectric slab can be truncated in plane for a discrete dark state. It was found that the discrete dark mode of the dielectric substrate can be excited with an electric resonator made of metallic structure for high-quality metamaterials. Later, the

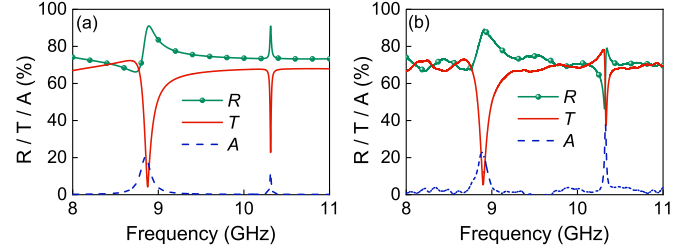


FIG. 2. (a) Calculated and (b) measured transmission, reflection, and absorption spectra for all-dielectric metamaterial with $p = 2$ mm.

high-quality metamaterial was demonstrated for lasing with low threshold, radiation damping tunability, directionality, and subwavelength integration. We investigate the interaction between the magnetic Mie resonance of a ceramic cuboid and the discrete dark mode of the dielectric substrate. The dispersion diagram of a uniform dielectric slab of thickness d (blue curve) and quantized dispersion of the composite dielectric-metal system (blue dots) is presented in Fig. 1(b). The E -field distribution of $TE_{2,0}$ mode is shown in Fig. 1(c). In Fig. 1(d), it can be found that the dark mode of the substrate or substrate mode can neither be excited by the incident wave nor be excited by the local field generated by the ceramic cuboid when it is placed in the center of the substrate. If we put the ceramic cuboid away from the center of the alumina slab, its magnetic mode will introduce asymmetry of the electric field distribution on the cross section of the waveguide. Once the magnetic resonance of the ceramic cuboid is excited directly by the magnetic component of the incident electromagnetic wave, the asymmetric distribution of electric field is no longer orthogonal to the discrete dark bound state ($TE_{2,0}$ mode) of the dielectric substrate, and thus the dark bound state can be excited with the magnetic dipole of the ceramic cuboid.

As discussed, the dark slab resonator can be excited by placing the ceramic cuboid away from center of cross section of the waveguide. We present in Fig. 2 the transmission, reflection, and absorption spectra of an all-dielectric metamaterial with cuboid position $p = 2$ mm. A typical Fano-shaped resonance [44–46] can be seen around 10.3 GHz. The sharp resonance is similar to the high Q excited with electric resonators [41]. The Q factor was extracted from the absorption spectrum as 356. To get a better understanding of the excitation of the substrate resonator, we present the calculated distribution of magnetic field at the resonant frequency (for the metamaterial with $p = 2$ mm, corresponding to the excited substrate resonance in Fig. 2) in Fig. 3. It can be seen that the magnetic field on the dielectric slab shows two nodes, which are close to the second discrete mode ($TE_{2,0}$) marked as the blue circle in Fig. 1(b). The magnetic field on the ceramic cuboid shows the picture of the magnetic dipolar mode, which induced the excitation of the substrate resonance. The H field in Fig. 3(b) confirms that the Fano-shaped resonance originates from the excitation of $TE_{2,0}$ mode of the alumina slab. The transmission and absorption spectra for different parameters p are presented in Fig. 4, and we note that the high- Q response of the substrate resonance can be further optimized to 648 when p is 0.5 mm.

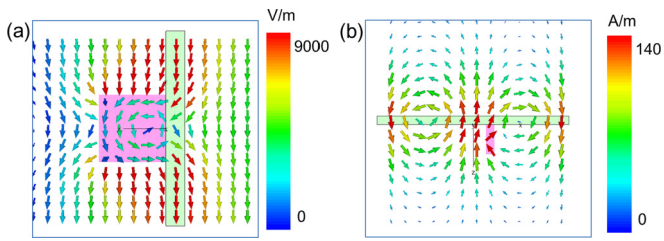


FIG. 3. Calculated electric field and magnetic field distributions on the cross section of the all-dielectric metamaterial (10.30 GHz), corresponding to the substrate resonance in Fig. 2).

After we have demonstrated the excitation of the substrate resonance with a typical Fano-shaped spectrum, we further adjust the resonant frequency of the magnetic mode of the dielectric cuboid to couple with the substrate resonance for EIT-like spectrum which usually needs two structured resonators. Here, we take the substrate resonance to replace another structured resonator and change the geometric parameters of the cuboid to $2.8 \times 2.8 \times 1.0$ mm based on numerical simulations. The measured absorption spectrum of the redesigned ceramic cuboid (placed at $p = 0$ mm) is shown in Fig. 5(a), the resonant frequency is 10.34 GHz, and the absorption at the resonant frequency is 30% with a Q factor of 87. Then we studied the electromagnetic properties of all-dielectric metamaterials in the case of the ceramic cuboid moved away from the center of the alumina slab,

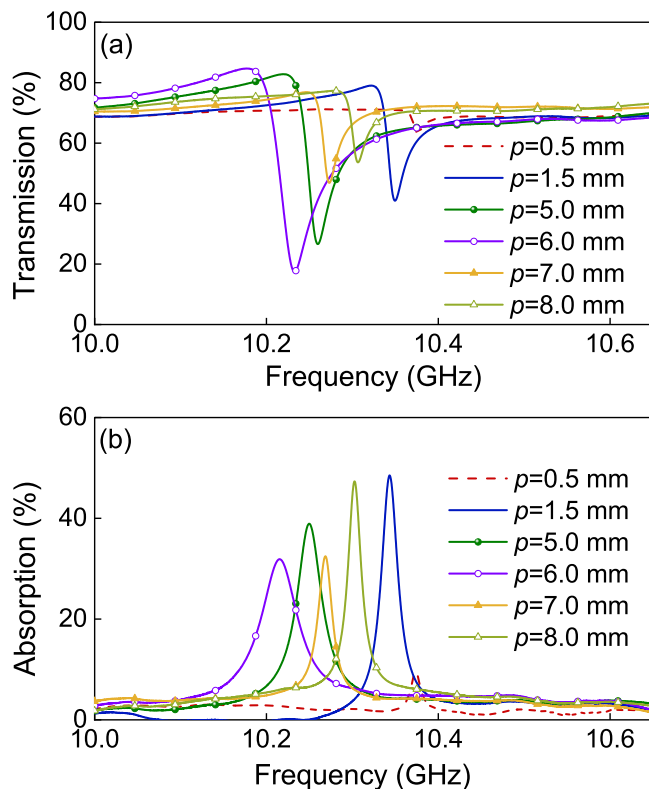


FIG. 4. Measured transmission (a) and absorption (b) spectra of dielectric cuboid with different positions.

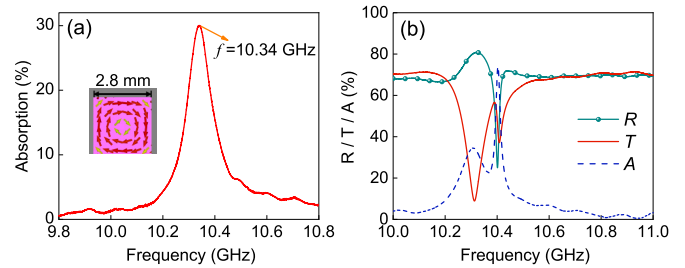


FIG. 5. (a) Absorption spectra of an all-dielectric metamaterial with ceramic cuboid size being $2.8 \text{ mm} \times 2.8 \text{ mm} \times 1.0 \text{ mm}$. (b) Transmission, reflection, and absorption spectra of an all-dielectric metamaterial with $p = 0.5 \text{ mm}$.

when the position was set as $p = 0.5 \text{ mm}$. Figure 5(b) shows the measured transmission, reflection, and absorption spectra. As can be seen, a transmission window appears within the resonance of the Mie resonance of the ceramic cuboid, which is just the picture of the EIT response.

The distributions of local electric field at the three typical frequencies of the EIT spectrum ($p = 0.5 \text{ mm}$) are presented in Fig. 6 for exploring the underlying physics of all-dielectric structure. For the two transmission dips, or absorption peaks, we can see that the local fields are mainly concentrated inside the ceramic cuboid. Strong field localization within the ceramic cuboid induced absorption enhancement (peak) on the spectrum. For the absorption dip, it is obvious that the magnetic Mie resonator is weakly excited, which is due to the destructive interference of the magnetic Mie resonance and substrate resonance. The EIT-like spectrum originates from the interference between the sharp substrate resonance of alumina slab and the relatively broad Mie resonance of the ceramic cuboid. The position of ceramic cuboid is a key factor in the excitation substrate resonance and the formation of EIT in our all-dielectric structure. Thus, we studied the influence of the position p on the EIT response. Based on the above study, we know that the two absorption peaks are due to the Mie resonance of ceramic cuboid and the substrate resonance, respectively. As can be seen from Fig. 5, the first absorption peak is mainly owing to the Mie resonance of cuboid. The frequency of magnetic Mie resonance of the cuboid originates from the inhomogeneous field of the waveguide mode in the experimental setup, which is similar to the results of previous study [47]. The EIT behavior can be significantly controlled by changing the position, as can be seen from

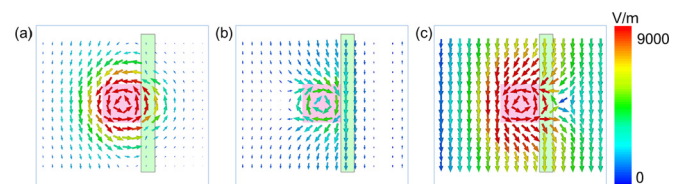


FIG. 6. Electric field distributions at the three typical frequencies of the EIT spectrum: (a) $f = 10.31 \text{ GHz}$, (b) $f = 10.39 \text{ GHz}$, and (c) $f = 10.41 \text{ GHz}$; the size of the ceramic cuboid is $2.8 \times 2.8 \times 1.0 \text{ mm}$.

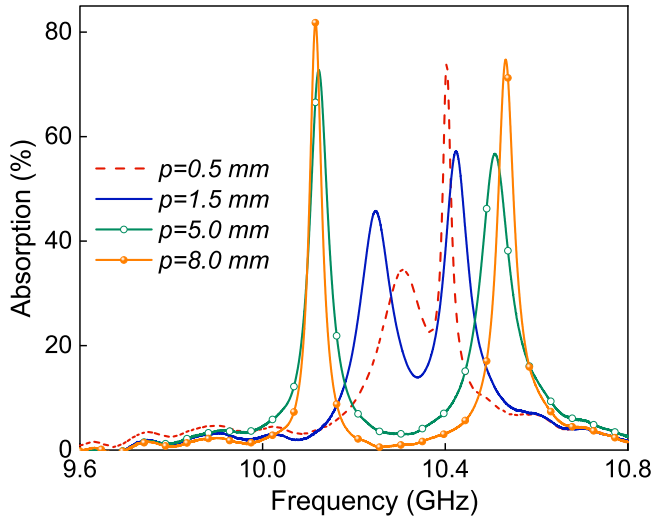


FIG. 7. Measured absorption spectra of all-dielectric metamaterials with ceramic cuboids of different position (the dimensions of the ceramic cuboid are $2.8 \times 2.8 \times 1.0$ mm).

the absorption spectra in Fig. 7. The absorption dip can be improved from 20% to 0% by changing $p = 0.5$ mm to $p = 8$ mm. In this process, the absorption peaks can also be modulation for two band absorbers. We can effectively regulate the absorption frequency and absorption intensity of the EIT-like effect by controlling the coupling between the magnetic Mie resonance and the substrate resonance. Based on these characteristics, the proposed all-dielectric metamaterial can be applied in microwave sensor and switching devices.

III. CONCLUSION

In summary, we have demonstrated the excitation of dark mode resonance of an alumina substrate or the substrate resonance, with the assistance of magnetic Mie resonance of a dielectric cuboid. Furthermore, the coupling between the bright resonance of the cuboid and guide mode resonance of the substrate was investigated for controllable EIT-like behavior. It is found that the absorption dip can be improved from 20% to 0% by controlling the coupling between the magnetic Mie resonance and the substrate resonance. Although our experiments were implemented in a waveguide configuration, the results can be extended to periodic metamaterial samples in free space [42]. The EIT-like spectrum demonstrated here can be simply tuned by changing only one dielectric resonator, given that the substrate resonance has many other ways to realize the transmission of waves, such as the Kerker effect [48–50]. Our results on the control of spectral response with dielectric structure coupled to the substrate resonance provide a way to realize optical mode coupling or control with all-dielectric metamaterials.

ACKNOWLEDGMENTS

The authors would like to acknowledge financial support from Natural Science Foundation of China (NSFC) (Grants No. 61771402, No. 11674266, and No. 61505164), Science and Technology Plan of Shenzhen City (No. JCYJ20170817162221169), Natural Science Foundation of Shaanxi Province (Programs No. 2018JM6024 and No. 2017JM6094), Shaanxi Province Postdoctoral Science Foundation (No. 2018BSHEDZZ64), Hong Kong Scholars Program (No. XJ2017006), and Fundamental Research Funds for the Central Universities (Grants No. 3102018jgc008 and No. 3102017zy033).

-
- [1] J. B. Pendry, *Phys. Rev. Lett.* **85**, 3966 (2000).
 - [2] R. A. Shelby, D. R. Smith, and S. Schultz, *Science* **292**, 77 (2001).
 - [3] D. R. Smith, J. B. Pendry, and M. C. K. Wiltshire, *Science* **305**, 788 (2004).
 - [4] S. Linden, C. Enkrich, M. Wegener, J. Zhou, T. Koschny, and C. M. Soukoulis, *Science* **306**, 1351 (2004).
 - [5] H. Chen, C. T. Chan, and P. Sheng, *Nat. Mater.* **9**, 387 (2010).
 - [6] C. M. Soukoulis and M. Wegener, *Nat. Photon.* **5**, 523 (2011).
 - [7] N. Liu, M. Hentschel, T. Weiss, A. P. Alivisatos, and H. Giessen, *Science* **332**, 1407 (2011).
 - [8] X. Yin, Z. Ye, J. Rho, Y. Wang, and X. Zhang, *Science* **339**, 1405 (2013).
 - [9] D. Lin, P. Fan, E. Hasman, and M. L. Brongersma, *Science* **345**, 298 (2014).
 - [10] N. Yu and F. Capasso, *Nat. Mater.* **13**, 139 (2014).
 - [11] X. Ding, F. Monticone, K. Zhang, L. Zhang, D. Gao, S. N. Burokur, A. de Lustrac, Q. Wu, C. Qiu, and A. Alu, *Adv. Mater.* **27**, 1195 (2015).
 - [12] A. Arbabi, Y. Horie, M. Bagheri, and A. Faraon, *Nat. Nanotechnol.* **10**, 937 (2015).
 - [13] K. Lan, J. Liu, Z. Li, X. Xie, W. Huo, Y. Chen, G. Ren, C. Zheng, D. Yang, S. Li *et al.*, *Matter Radiat. Extremes* **1**, 8 (2018).
 - [14] E. Campbell, V. Goncharov, T. Sangster, S. Regan, P. Radha, R. Betti, J. Myatt, D. Froula, M. Rosenberg, I. Igumenshchev *et al.*, *Matter Radiat. Extremes* **2**, 37 (2018).
 - [15] M. Murakami and D. Nishi, *Matter Radiat. Extremes* **2**, 55 (2018).
 - [16] S. E. Harris, *Phys. Rev. Lett.* **62**, 1033 (1989).
 - [17] L. V. Hau, S. E. Harris, Z. Dutton, and C. H. Behroozi, *Nature (London)* **397**, 594 (1999).
 - [18] S. Zhang, D. A. Genov, Y. Wang, M. Liu, and X. Zhang, *Phys. Rev. Lett.* **101**, 047401 (2008).
 - [19] N. Papasimakis, V. A. Fedotov, N. I. Zheludev, and S. L. Prosvirnin, *Phys. Rev. Lett.* **101**, 253903 (2008).
 - [20] P. Tassin, L. Zhang, T. Koschny, E. N. Economou, and C. M. Soukoulis, *Phys. Rev. Lett.* **102**, 053901 (2009).
 - [21] P. Tassin, L. Zhang, T. Koschny, E. N. Economou, and C. M. Soukoulis, *Opt. Express* **17**, 5595 (2009).
 - [22] N. Papasimakis, Y. Fu, V. A. Fedotov, S. L. Prosvirnin, D. P. Tsai, and N. I. Zheludev, *Appl. Phys. Lett.* **94**, 211902 (2009).

- [23] H. Cheng, S. Chen, P. Yu, X. Duan, B. Xie, and J. Tian, *Appl. Phys. Lett.* **103**, 203112 (2013).
- [24] F. Zhang, Q. Zhao, C. Lan, X. He, W. Zhang, J. Zhou, and K. Qiu, *Appl. Phys. Lett.* **104**, 131907 (2014).
- [25] Y. Fan, T. Qiao, F. Zhang, Q. Fu, J. Dong, B. Kong, and H. Li, *Sci. Rep.* **7**, 40441 (2017).
- [26] P. Tassin, L. Zhang, R. Zhao, A. Jain, T. Koschny, and C. M. Soukoulis, *Phys. Rev. Lett.* **109**, 187401 (2012).
- [27] R. Yahiaoui, M. Manjappa, Y. K. Srivastava, and R. Singh, *Appl. Phys. Lett.* **111**, 021101 (2017).
- [28] J. Xu, Y. Fan, R. Yang, Q. Fu, and F. Zhang, *Opt. Express* **27**, 2837 (2019).
- [29] A. Ahmadi and H. Mosallaei, *Phys. Rev. B* **77**, 045104 (2008).
- [30] Q. Zhao, J. Zhou, F. Zhang, and D. Lippens, *Mater. Today* **12**, 60 (2009).
- [31] F. Zhang, L. Kang, Q. Zhao, J. Zhou, and D. Lippens, *New J. Phys.* **14**, 033031 (2012).
- [32] P. Moitra, Y. M. Yang, Z. Anderson, I. I. Kravchenko, D. P. Briggs, and J. Valentine, *Nat. Photon.* **7**, 791 (2013).
- [33] F. Zhang, Q. Zhao, J. Zhou, and S. Wang, *Opt. Express* **21**, 19675 (2013).
- [34] Y. Yang, I. I. Kravchenko, D. P. Briggs, and J. Valentine, *Nat. Commun.* **5**, 5753 (2014).
- [35] F. Zhang, X. Huang, Q. Zhao, L. Chen, Y. Wang, Q. Li, X. He, C. Li, and K. Chen, *Appl. Phys. Lett.* **105**, 172901 (2014).
- [36] Q. Zhao, Z. Xiao, F. Zhang, J. M. Ma, M. Qiao, Y. Meng, C. Lan, B. Li, J. Zhou, P. Zhang *et al.*, *Adv. Mater.* **27**, 6187 (2015).
- [37] S. Jahani and Z. Jacob, *Nat. Nanotechnol.* **11**, 23 (2016).
- [38] W. Zhu, R. Yang, Y. Fan, Q. Fu, H. Wu, P. Zhang, N. Shen, and F. Zhang, *Nanoscale* **10**, 12054 (2018).
- [39] X. Sun, Q. Fu, Y. Fan, H. Wu, K. Qiu, R. Yang, W. Cai, and F. Zhang, *Sci. Rep.* **9**, 5417 (2019).
- [40] W. Wang, L. Zheng, and J. Qi, *Appl. Phys. Express* **12**, 075002 (2019).
- [41] A. Jain, P. Tassin, T. Koschny, and C. M. Soukoulis, *Phys. Rev. Lett.* **112**, 117403 (2014).
- [42] S. Droulias, A. Jain, T. Koschny, and C. M. Soukoulis, *Phys. Rev. Lett.* **118**, 073901 (2017).
- [43] S. Droulias, T. Koschny, and C. M. Soukoulis, *ACS Photon.* **5**, 3788 (2018).
- [44] N. Verellen, Y. Sonnefraud, H. Sobhani, F. Hao, V. V. Moshchalkov, P. Van Dorpe, P. Nordlander, and S. A. Maier, *Nano Lett.* **9**, 1663 (2009).
- [45] B. Luk'yanchuk, N. I. Zheludev, S. A. Maier, N. J. Halas, P. Nordlander, H. Giessen, and C. T. Chong, *Nat. Mater.* **9**, 707 (2010).
- [46] Q. Fu, F. Zhang, Y. Fan, X. He, T. Qiao, and B. Kong, *Opt. Express* **24**, 1708 (2016).
- [47] F. Zhang, C. Li, Y. Fan, R. Yang, N.-H. Shen, Q. Fu, W. Zhang, Q. Zhao, J. Zhou, T. Koschny *et al.*, *Adv. Mater.* **31**, 1903206 (2019).
- [48] V. E. Babicheva and A. B. Evlyukhin, *Laser Photon. Rev.* **11**, 1700132 (2017).
- [49] M. Dubois, L. Leroi, Z. Raolison, R. Abdeddaim, T. Antonakakis, J. De Rosny, A. Vignaud, P. Sabouroux, E. Georget, B. Larrat *et al.*, *Phys. Rev. X* **8**, 031083 (2018).
- [50] W. Liu and Y. S. Kivshar, *Opt. Express* **26**, 13085 (2018).